

# **DOUBLE PENDULUM: NORMAL MODES AND CHAOS**

*A project submitted for the evaluation of*  
**INTEGRATED PHYSICS LABORATORY in SEM-VII**

*by*  
**ADHILSHA A (2011006)**



*to the*  
**School of Physical Sciences**  
**National Institute of Science Education and Research**  
**Bhubaneswar**  
**November 26, 2023**

## ABSTRACT

We have known the double pendulum as a system that proves to be both theoretically and experimentally rich, despite its simplicity with only two moving parts and two axles. Our experiments focused on exploring different faces of the system's linear and nonlinear behaviour. Key parameters under scrutiny include the normal mode frequencies ( $\omega_{1,2}$ ) in the linear mode and the Lyapunov exponent ( $\lambda$ ) related to the chaos of the double pendulum. We obtained the normal mode frequencies closely following the analytically predicted normal mode frequencies. We also obtained a positive Lyapunov exponent indicating definite chaos in the double pendulum.

# Contents

<b>1</b>	<b>Introduction</b>	<b>1</b>
<b>2</b>	<b>Theory</b>	<b>2</b>
2.1	Chaos in double pendulum . . . . .	2
2.2	General Motion . . . . .	3
2.3	Small Angle Motion . . . . .	5
2.4	Lyapunov exponent ( $\lambda$ ) . . . . .	6
<b>3</b>	<b>Experimental Setup</b>	<b>8</b>
<b>4</b>	<b>Experimental Methods</b>	<b>10</b>
4.1	Data Collection . . . . .	10
4.2	Data Analysis . . . . .	10
4.2.1	Video to Data . . . . .	10
4.2.2	Normal modes . . . . .	11
4.2.3	Chaos . . . . .	12
<b>5</b>	<b>Observations and Calculation</b>	<b>13</b>
5.1	Normal mode (analytical) . . . . .	13
5.2	Normal mode (experimental) . . . . .	14
5.3	Chaos . . . . .	16
5.4	Error Analysis . . . . .	18
<b>6</b>	<b>Results</b>	<b>19</b>
<b>7</b>	<b>Discussions</b>	<b>20</b>
7.1	Sources of error . . . . .	24
7.2	Precautions . . . . .	24
<b>8</b>	<b>Conclusions</b>	<b>26</b>
<b>References</b>		<b>27</b>
<b>Appendix A</b>		<b>28</b>

# List of Figures

2.1	Schematic of double pendulum . . . . .	3
2.2	Two normal mode trajectories, NM1 and NM2, in a double pendulum	6
3.1	Front profile of the setup . . . . .	9
3.2	Side profile of the setup . . . . .	9
5.1	Analytically predicted NM1 trajectory . . . . .	14
5.2	FFT of analytically predicted $\theta_1$ for NM1 . . . . .	14
5.3	Analytically predicted NM2 trajectory . . . . .	14
5.4	FFT of analytically predicted $\theta_1$ for NM2 . . . . .	14
5.5	Experimental NM1 trajectory . . . . .	15
5.6	FFT of experimental $\theta_1$ for NM1 . . . . .	15
5.7	Experimental NM2 trajectory . . . . .	15
5.8	FFT of experimental $\theta_1$ for NM2 . . . . .	15
5.9	Mixed NM1&NM2 trajectory . . . . .	15
5.10	FFT of $\theta_1$ for mixed NM1&NM2 . . . . .	15
5.11	Visualizaton of trajectory divergence from $(90^\circ, 0^\circ)$ initial angles . . . . .	17
5.12	Sample of Lyapunov exponent from $(90^\circ, 0^\circ)$ initial angles . . . . .	17
5.13	Visualizaton of trajectory divergence from $(90^\circ, 180^\circ)$ initial angles . . . . .	17
5.14	Sample of Lyapunov exponent from $(90^\circ, 180^\circ)$ initial angles . . . . .	17
5.15	Visualizaton of trajectory divergence from $(170^\circ, 0^\circ)$ initial angles . . . . .	17
5.16	Sample of Lyapunov exponent from $(170^\circ, 0^\circ)$ initial angles . . . . .	17
7.1	Before applying hann window . . . . .	21
7.2	After applying hann window . . . . .	21
A.1	NM1 trial 1 FFT . . . . .	28
A.2	NM1 trail 1 trajectory . . . . .	28
A.3	NM1 trial 2 FFT . . . . .	29
A.4	NM1 trial 2 trajectory . . . . .	29
A.5	NM2 trial 1 FFT . . . . .	29
A.6	NM2 trial 1 trajectory . . . . .	29
A.7	NM2 trial 2 FFT . . . . .	29
A.8	NM2 trial 2 trajectory . . . . .	29
A.9	$(90^\circ, 0^\circ)$ trial 11 vs 13 . . . . .	30
A.10	$(90^\circ, 0^\circ)$ trial 11 vs 14 . . . . .	30
A.11	$(90^\circ, 0^\circ)$ trial 11 vs 15 . . . . .	30
A.12	$(90^\circ, 0^\circ)$ trial 13 vs 15 . . . . .	30
A.13	$(90^\circ, 0^\circ)$ trial 14 vs 15 . . . . .	30
A.14	$(90^\circ, 180^\circ)$ trial 31 vs 38 . . . . .	30
A.15	$(90^\circ, 180^\circ)$ trial 31 vs 39 . . . . .	31
A.16	$(90^\circ, 180^\circ)$ trial 31 vs 41 . . . . .	31
A.17	$(90^\circ, 180^\circ)$ trial 38 vs 39 . . . . .	31
A.18	$(90^\circ, 180^\circ)$ trial 39 vs 41 . . . . .	31
A.19	$(170^\circ, 0^\circ)$ trial 52 vs 52 . . . . .	31
A.20	$(170^\circ, 0^\circ)$ trial 52 vs 55 . . . . .	31

*LIST OF FIGURES*

---

A.21 (170°,0°) trial 52 vs 58 . . . . .	32
A.22 (170°,0°) trial 54 vs 55 . . . . .	32
A.23 (170°,0°) trial 54 vs 47 . . . . .	32
A.24 (170°,0°) trial 54 vs 58 . . . . .	32
A.25 (170°,0°) trial 57 vs 58 . . . . .	32

# Chapter 1

## Introduction

The double pendulum has been extensively studied due to its interesting behavior, even though it's a simple setup. From its basic structure to its applications in biomechanics, the essential characteristics of the double pendulum are relevant across various fields. This system can display both linear and nonlinear behavior, depending on its initial state.

A crucial aspect of the double pendulum is its behavior in chaotic cases. When the system starts from slightly different points, the two-time evolutions deviate exponentially over time. This leads to significant consequences for the system's overall time evolution. This deviation rate between two similar yet slightly different starting conditions can be measured. Interestingly, this phenomenon is related to the challenge of making reliable weather predictions beyond a certain timescale by weather forecasters.

We conduct our experiment with the following objectives:

1. To study the double pendulum system, formulate related equations of motion for a numerical solution.
2. To stimulate normal modes in the double pendulum system and measure the normal mode frequencies experimentally and compare it to analytically predicted normal mode frequencies.
3. To confirm the chaotic behavior present in the double pendulum using Lyapunov's exponent.

# Chapter 2

## Theory

The double pendulum system under analysis exhibits both linear and non-linear behaviour depending on the initial state of the system. The linear behaviour in the double pendulum, observed in small angles, contains the characteristic normal mode frequencies. The double pendulum shows chaotic behaviour in large angles. The key characteristic is that the trajectories that start from the near initial conditions diverge from each other exponentially in such cases.

### 2.1 Chaos in double pendulum

In physics, Chaos theory focuses on systems that, in theory, should be predictable because they follow specific rules. However, in practice, these systems seem predictable for a while, and then they 'seem' to continue randomly.

The reason it's hard to predict chaotic systems is that small uncertainties build up over time. This makes points in the system that start close together quickly move far apart, making it tricky to study, especially when doing experiments.

To be considered chaotic, a system needs to meet specific conditions. There are various ways to define chaos, and our system meets most of these definitions. The most common definition is:

1. *Extreme sensitivity to initial conditions*: This means that even a slight deviation from the starting point leads to significantly different outcomes. This is shown later through the results.

2. *Topological transitivity*: It's a technical definition not crucial for our case as the mathematical requirement can't be measured experimentally with our apparatus.
3. *Dense periodic orbit*: Dense implies that given a point in phase space, there is a point in a periodic orbit (a curve that after some time again comes back to the same point) infinitesimally close to it, this ensures that there is a lot of aperiodic behavior in our system. This is the case in the double pendulum system.

## 2.2 General Motion

The physical double pendulum we used for the experiment was closely approximated to the following. The double pendulum consists of two pendulum rods, the first one with a fixed pivot point, whereas the second rod is attached at the end of the first. Each rod is assumed to have a uniformly distributed mass. The rods have lengths  $l_1$ ,  $l_2$  and masses  $m_1$ ,  $m_2$  for the upper and lower rods respectively. The centers of mass of the rods are at  $(x_1, y_1)$  and  $(x_2, y_2)$ , which is at the middle of each rod. This system is depicted in Figure 2.1.

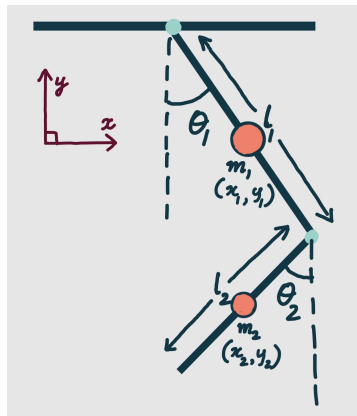


Figure 2.1: Schematic of double pendulum

Now, the centers of masses  $(x_1, y_1)$  and  $(x_2, y_2)$  are given by:

$$\begin{aligned} (x_1, y_1) &= \left( \frac{l_1}{2} \sin \theta_1, -\frac{l_1}{2} \cos \theta_1 \right) \\ (x_2, y_2) &= \left( l_1 \sin \theta_1 + \frac{l_2}{2} \sin \theta_2, -l_1 \cos \theta_1 - \frac{l_2}{2} \cos \theta_2 \right) \end{aligned}$$

Taking the derivatives, we get:

$$\begin{aligned} (\dot{x}_1, \dot{y}_1) &= \left( \frac{l_1}{2} \dot{\theta}_1 \cos \theta_1, \frac{l_1}{2} \dot{\theta}_1 \sin \theta_1 \right) \\ (\dot{x}_2, \dot{y}_2) &= \left( l_1 \dot{\theta}_1 \cos \theta_1 + \frac{l_2}{2} \dot{\theta}_2 \cos \theta_2, l_1 \dot{\theta}_1 \sin \theta_1 + \frac{l_2}{2} \dot{\theta}_2 \sin \theta_2 \right) \end{aligned} \quad (2.1)$$

Now, we can find the total kinetic energy  $T$  as the sum of translational kinetic energies of the centers of mass, given by  $\frac{1}{2}m_i(\dot{x}_i^2 + \dot{y}_i^2)$ . The angular part of the kinetic energy about the center of mass, which is  $I_i = \frac{m_il_i^2}{12}$ . Thus, the total kinetic energy  $T$  and the potential energy  $V$  are given by:

$$\begin{aligned} T &= \frac{1}{2}m_1(\dot{x}_1^2 + \dot{y}_1^2)^2 + \frac{1}{2}m_2(\dot{x}_2^2 + \dot{y}_2^2)^2 + \frac{1}{2}I_1\dot{\theta}_1^2 + \frac{1}{2}I_2\dot{\theta}_2^2 \\ V &= m_1gy_1 + m_2gy_2 \end{aligned} \quad (2.2)$$

Substituting with equations (2.1), we get the reduced equations:

$$\begin{aligned} T &= \frac{1}{2}J_a\dot{\theta}_1^2 + \frac{1}{2}J_b\dot{\theta}_2^2 + J_x\dot{\theta}_1\dot{\theta}_2 \cos(\theta_2 - \theta_1) \\ V &= -\mu_1 \cos \theta_1 - \mu_2 \cos \theta_2 \end{aligned} \quad (2.3)$$

where the constants are defined as:

$$\begin{aligned} J_a &= \frac{1}{3}m_1l_1^2 + m_2l_1^2 \\ J_b &= \frac{1}{3}m_2l_2^2 \\ J_x &= \frac{1}{2}m_2l_1l_2 \\ \mu_1 &= \left( \frac{1}{2}m_1 + m_2 \right) gl_1 \\ \mu_2 &= \frac{1}{2}m_2gl_2 \end{aligned} \quad (2.4)$$

With the Lagrangian as  $\mathcal{L} = T - V$ , we can calculate the equations of motion (EoM) for the double pendulum using Euler-Lagrange equations,  $\frac{d}{dt} \left( \frac{\delta \mathcal{L}}{\delta \dot{q}_i} \right) - \frac{\delta \mathcal{L}}{\delta q_i} = 0$

for  $q_i = \theta_1, \theta_2$ . Applying the equations together, we get EoM as:

$$\begin{aligned} J_a \ddot{\theta}_1 + J_x \cos(\theta_2 - \theta_1) \ddot{\theta}_2 - J_x \sin(\theta_2 - \theta_1) \dot{\theta}_2^2 + \mu_1 \sin \theta_1 &= 0 \\ J_b \ddot{\theta}_2 + J_x \cos(\theta_2 - \theta_1) \ddot{\theta}_1 + J_x \sin(\theta_2 - \theta_1) \dot{\theta}_1^2 + \mu_2 \sin \theta_2 &= 0 \end{aligned} \quad (2.5)$$

This set of equations can be transformed into coupled first-order DE for solving it numerically. These coupled ODEs we obtained are:

$$\begin{aligned} \frac{d\theta_1}{dt} &= \dot{\theta}_2 \\ \frac{d\theta_2}{dt} &= \dot{\theta}_1 \\ \frac{d\omega_1}{dt} &= \frac{\frac{J_x^2}{2J_b} \sin(2\theta_2 - 2\theta_1) \dot{\theta}_1^2 + \frac{J_x \mu_2}{J_b} \sin \theta_2 \cos(\theta_2 - \theta_1) + J_x \sin(\theta_2 - \theta_1) \dot{\theta}_2^2 - \mu_1 \sin \theta_1}{J_a - \frac{J_x^2}{J_b} \cos^2(\theta_2 - \theta_1)} \\ \frac{d\omega_1}{dt} &= \frac{-\frac{J_x^2}{2J_a} \sin(2\theta_2 - 2\theta_1) \dot{\theta}_1^2 + \frac{J_x \mu_1}{J_a} \sin \theta_1 \cos(\theta_2 - \theta_1) - J_x \sin(\theta_2 - \theta_1) \dot{\theta}_1^2 - \mu_2 \sin \theta_2}{J_b - \frac{J_x^2}{J_a} \cos^2(\theta_2 - \theta_1)} \end{aligned} \quad (2.6)$$

These equations can be fed into the Runge-Kutta 4<sup>th</sup> order (RK4) algorithm for solving the double pendulum motion analytically.

## 2.3 Small Angle Motion

The complete derivation is long, and hence the details are omitted. The core of the derivation is from Levien and Tan (1993) [1]. We take the Lagrangian  $\mathcal{L}$  from equations (2.3) and apply the small angle approximations. The resulting Lagrangian and EoM are obtained as:

$$\mathcal{L} = \frac{1}{2} J_a \dot{\theta}_1^2 + \frac{1}{2} J_b \dot{\theta}_2^2 + J_x \dot{\theta}_1 \dot{\theta}_2 + \mu_1 \left( 1 - \frac{\theta_1^2}{2} \right) + \mu_2 \left( 1 - \frac{\theta_2^2}{2} \right) \quad (2.7)$$

$$\begin{aligned} J_a \ddot{\theta}_1 + J_x \ddot{\theta}_2 - \mu_1 \theta_1 &= 0 \\ J_b \ddot{\theta}_2 + J_x \ddot{\theta}_1 - \mu_2 \theta_2 &= 0 \end{aligned} \quad (2.8)$$

In matrix form, we write it as:

$$\begin{bmatrix} J_a & J_x \\ J_x & J_b \end{bmatrix} \begin{bmatrix} \ddot{\theta}_1 \\ \ddot{\theta}_2 \end{bmatrix} + \begin{bmatrix} -\mu_1 & 0 \\ 0 & -\mu_2 \end{bmatrix} \begin{bmatrix} \theta_1 \\ \theta_2 \end{bmatrix} = \mathbf{0} \quad (2.9)$$

Considering this equation in the form  $\mathbf{M}\ddot{\Theta} + \mathbf{K}\Theta = \mathbf{0}$  and the solution is given by:

$$|\mathbf{K} - \omega^2\mathbf{M}| = 0 \quad (2.10)$$

The solution is of the form:

$$\Theta = \begin{bmatrix} \theta_1 \\ \theta_2 \end{bmatrix} = \begin{bmatrix} A_1 \\ A_2 \end{bmatrix} e^{i\omega_1 t} + \begin{bmatrix} B_1 \\ B_2 \end{bmatrix} e^{i\omega_2 t} \quad (2.11)$$

Solving this, we get the normal mode frequencies as:

$$\omega_{1,2}^2 = \frac{-(\mu_1 J_b + J_a \mu_2) \pm \sqrt{(\mu_1 J_b + J_a \mu_2)^2 + 4(J_x^2 - J_a J_b)\mu_1 \mu_2}}{2(J_x^2 - J_a J_b)} \quad (2.12)$$

The two normal modes in a double pendulum, Normal mode 1 (NM1) with frequency  $\omega_1$  and Normal mode 2 (NM2) with frequency  $\omega_2$ , are depicted in Figure 2.2. If any arbitrary perturbation, assuming the small angle limit is maintained, it can be expressed as a linear superposition of the two normal modes.

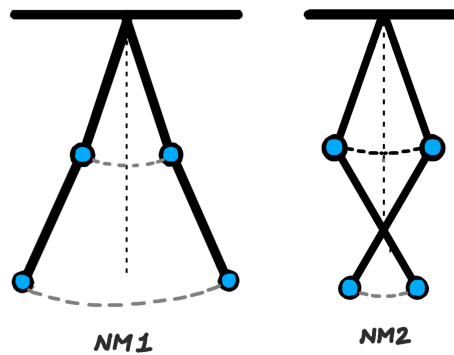


Figure 2.2: Two normal mode trajectories, NM1 and NM2, in a double pendulum

## 2.4 Lyapunov exponent ( $\lambda$ )

The Lyapunov exponent characterizes the exponential rate of divergence or convergence of nearby trajectories, thus studying the system's sensitivity to the initial state.

Mathematically, it is defined as:

$$d_t = d_0 e^{\lambda t} \quad (2.13)$$

where  $d_0$  is the initial separation between the nearby trajectories at  $t = 0$ ,  $\lambda$  is the Lyapunov exponent, and  $d_t$  is the separation between these trajectories at time  $t$ .

It's crucial to emphasize that this  $d_0$  value needs to be extremely small to qualify as the Lyapunov exponent. Achieving this condition experimentally poses significant challenges, particularly in our setup, where maintaining the absolute stillness of the pendulum arms with precisely the same angle is practically unattainable. Due to this deviation from the ideal, the exponential behavior is only local and gradually transitions into non-exponential behavior over a short period.

Since the Lyapunov exponent needs to be evaluated for  $d_0 \rightarrow 0$  and it is experimentally difficult to attain, we will look at the exponent qualitatively in our measurements. For the system to be chaotic, the Lyapunov exponent should be *positive*, and that is where our focus is.

- If  $\lambda < 0$ , trajectories in phase space are converging toward each other, indicating that the system is dissipative. This aligns with our expectations, as in dissipative systems, the separation between distinct phase space trajectories diminishes over time as the overall motion of the system loses energy, like in dissipative SHM.
- If  $\lambda = 0$ , the distances between trajectories will remain constant. A classic example illustrating this is simple harmonic motion (SHM). In SHM, the paths in phase space form circular orbits that remain a consistent separation between them.
- If  $\lambda > 0$ , the orbits in phase space will exponentially diverge from each other. This behavior indicates, though not a definitive proof, chaos in the system.

# Chapter 3

## Experimental Setup

The double pendulum system in the laboratory was designed based on the Myers et. al. (2020) [2]. The double pendulum apparatus have the following components:

- Two arms of the upper rod (Length - 12", Width - 1.5", thickness - 0.375")
- Bottom rod (Length - 9", Width - 1.5", thickness - 0.375")
- Pivot (Inner radius - 0.166", Outer radius - 0.375")
- Spacing block (Length - 1.5", Width - 1.5" and Thickness - 0.65")
- Screws (various diameters and lengths)
- Bearings for axles ( $\times 3$ ) - McMaster-CARR 60355k14
- Collars ( $\times 2$ ) - McMaster-CARR 6166K23
- Aluminium profile for support
- Tracking markers - circular colored paper pasted at the end of each rod

The other components we used for measurement include:

- Camera device (1080p 60fps)
- Tripod for mounting the camera device.
- PC/Laptop with the software *Tracker* [3] and the python environment to run analysis.

The experimental setup is shown in Figures 3.1 and 3.2.



Figure 3.1: Front profile of the setup



Figure 3.2: Side profile of the setup

# Chapter 4

## Experimental Methods

### 4.1 Data Collection

- The normal mode motions shown in Figure 2.2 are practically replicated in the double pendulum system. The angles are kept as small as possible.
- To produce chaos in the double pendulum, the system is initialized at large angles. We used three initial angles  $(\theta_1, \theta_2) \approx [(90^\circ, 0^\circ), (90^\circ, 180^\circ), (170^\circ, 0^\circ)]$ .
- Multiple trials of each setting are recorded by placing the camera in front of the system.

### 4.2 Data Analysis

#### 4.2.1 Video to Data

- By setting the appropriate coordinate system with the origin on the top pivot and registering the markers on both rods on the Tracker software, we track the movement of the double pendulum.
- We obtain the time series data including the time and coordinates of each marker i.e.  $(t, x_1, y_1, x_2, y_2)$ . Note that these are not the center of mass coordinates but the coordinates of the end of both rods, where markers were placed.
- Exporting this data as a txt file into the Python environment, we use the `numpy`, `scipy`, `scikit` and other libraries for further analysis.

- We use `np.arctan2(x1, y1)` to get  $\theta_1$  and `np.arctan2(x2 - x1, y2 - y1)` to get  $\theta_2$  and convert them to degrees using `np.degrees()`. The obtained  $\theta_i$  values are in (-180°, 180°) range.
- We extend this to (-∞, ∞) range by detecting when the trajectory crosses the boundaries (-180°, 180° values) and correcting the consecutive values to ensure continuity. For chaos analysis, we need to make sure of this continuity even in the initial initial condition. The reasoning is discussed later in Chapter 7.
- Then, we can use `np.gradient(θi)` to get  $\omega_i$  and set the initial  $\omega_i$  values to zero under the assumption it starts from the still position.

#### 4.2.2 Normal modes

- For the normal mode analysis, we consider the first 600 frames (10 seconds) from the moment of release (or from the next oscillation that reaches the same point).
- We apply the Hann window (`hann()` from `scikit.signal.windows`) on  $\theta_i$  from the video analysis to optimize it for FFT analysis whose reasoning is later explained in Chapter 7.
- The modified ( $\theta_1, \theta_2$ ) values are then passed to `fft()` and  $t$  through `fftfreq()` (both from `scikit` library) to find the FFT Amplitude vs frequency graph whose peaks gives us the normal mode frequencies.
- We take the average over multiple trials (within small angle limit of 15°) for each normal mode to get the final values.

### 4.2.3 Chaos

- We analyzed the initial 30 frames from the moment of release as the frame rate is 60 per second. The reasoning is discussed in Section 7.
- To find the phase space difference between two near trajectories, we calculate the phase space from their respective  $\theta_1, \theta_2, \omega_1$ , and  $\omega_2$  values.

$$\phi_i = \sqrt{\theta_1^2 + \theta_2^2 + \omega_1^2 + \omega_2^2} \quad (4.1)$$

- We can find the required phase space difference as:

$$d = |\phi_1 - \phi_2| \quad (4.2)$$

- We use the `curvefit()` from `scipy.optimize` on exponential function and the calculated  $d(t)$ . We put a strong limit on  $d_0$  value and calculate the optimized  $\lambda$  value and its error from the `curvefit()`.
- We take the weighted average of the  $\lambda$  from multiple trials of each setting to find the final values.

# Chapter 5

## Observations and Calculation

### 5.1 Normal mode (analytical)

We use equations (2.8) and program it into Python functions. Then, feed it to the RK4 algorithm along with the defined constants given below.

```
1 # CONSTANTS
2 g = np.float64(9.80665) # m/s^2 acceleration due to gravity
3 m1 = np.float64(2 * 0.3048 * 0.0381 * 0.009525 * 2710) # kg -
4     mass of upper rod
5 m2 = np.float64(0.2286 * 0.0381 * 0.009525 * 2710) # kg -
6     mass of lower rod
7 l1 = np.float64(0.3048) # m - length of upper rod
8 l2 = np.float64(0.2286) # m - length of lower rod
9
10 NM1_ratio = 3.5 / 2 # theta2 / theta1 ratios
11 NM2_ratio = -6.8 / 2
12 # found by trial and error
13
14 # initial theta1, theta2 values
15 t1i = np.float64(radians(2))
16 t2i = t1i * NM1_ratio # change to NM2_ratio for NM2
```

**N.B.** For all the observations regarding Normal modes, we found that the FFT for  $\theta_1$  and  $\theta_2$  yielded the same frequency peaks. So, we will only be presenting the  $\theta_1$  FFT peaks.

The NM1 trajectory and its frequency are given in Figures 5.1 and 5.2, whereas the NM2 trajectory and its frequency are given in Figures 5.3 and 5.4. From these, we get the analytically predicted Normal mode frequencies:

$$\omega_1 = 0.88 \text{ Hz}$$

$$\omega_2 = 1.86 \text{ Hz}$$

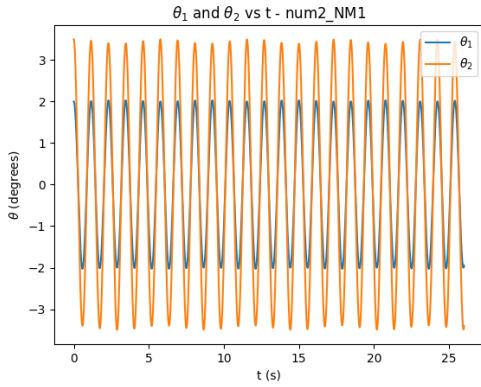


Figure 5.1: Analytically predicted NM1 trajectory

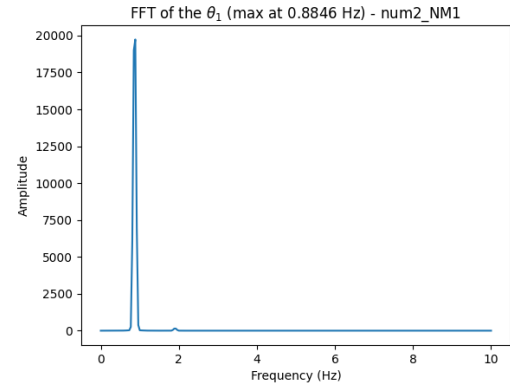


Figure 5.2: FFT of analytically predicted  $\theta_1$  for NM1

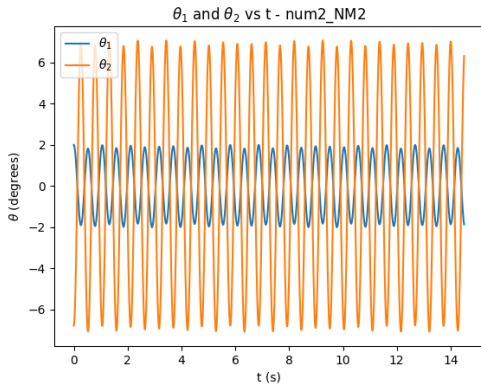


Figure 5.3: Analytically predicted NM2 trajectory

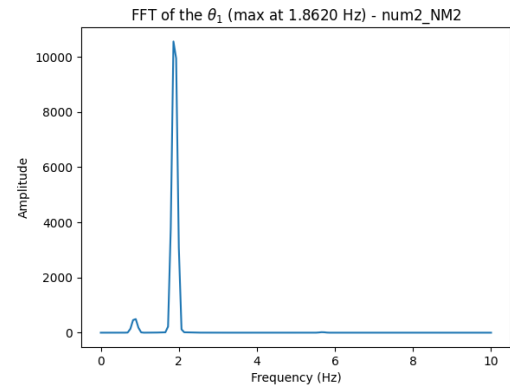


Figure 5.4: FFT of analytically predicted  $\theta_1$  for NM2

## 5.2 Normal mode (experimental)

Following the experimental method, we replicated both normal modes to the best of our abilities and demonstrated a mixed mode. See Figures 5.5 to 5.10 for a sample of each. The rest of the graphs are added to the Appendix. From there, we get the experimental values of normal mode frequencies:

$$\omega_1 = (0.902 \pm 0.006) \text{ Hz}$$

$$\omega_2 = (1.801 \pm 0.006) \text{ Hz}$$

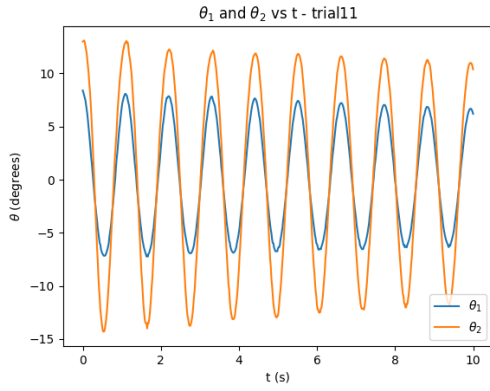


Figure 5.5: Experimental NM1 trajectory

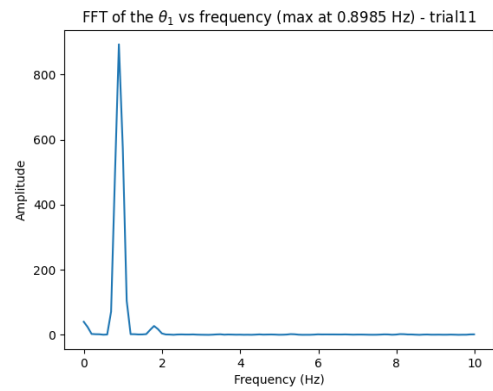


Figure 5.6: FFT of experimental  $\theta_1$  for NM1

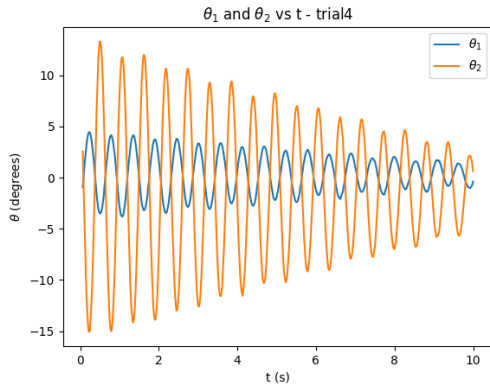


Figure 5.7: Experimental NM2 trajectory

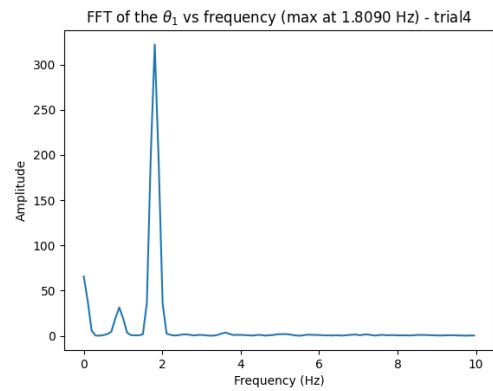


Figure 5.8: FFT of experimental  $\theta_1$  for NM2

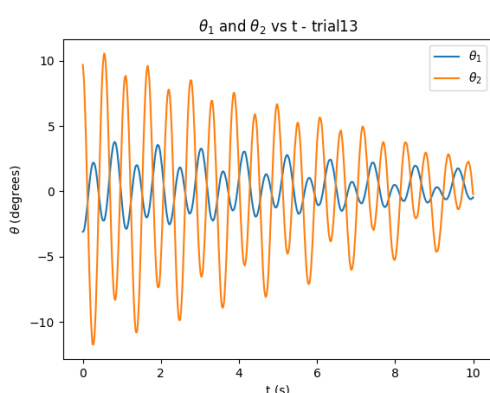


Figure 5.9: Mixed NM1&NM2 trajectory

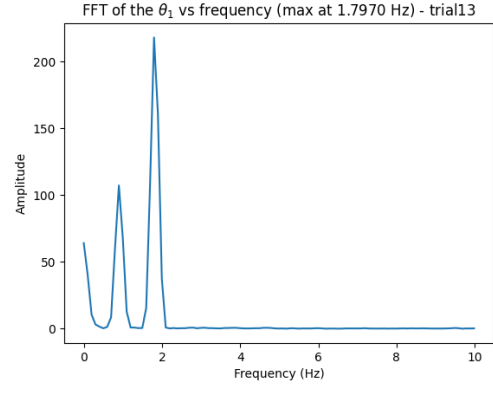


Figure 5.10: FFT of  $\theta_1$  for mixed NM1&NM2

### 5.3 Chaos

For the analysis of chaos, we have done more than 25 trials across all settings and filtered the proper ones, as some of them contained significant deviations due to the experimental errors involved.

To show the chaotic behavior in all three settings we chose, we are showing the combined divergence of trajectories visually. We also show a sample of the exponential rate of divergence of trajectories for each setting. *Note that the y-axis is in semi-log scale, hence expected to be seen a linear trend in given graphs.* See Figures 5.11 to 5.16.

For the trials starting from  $(90^\circ, 0^\circ)$  initial angles, the trajectory divergence is visually represented in Figure 5.11, and a sample of Lyapunov exponent is shown in Figure 5.12. We get the average value from trials:

$$\lambda_{(90,0)} = (20.4 \pm 0.4)$$

For the trials starting from  $(90^\circ, 180^\circ)$  initial angles, the trajectory divergence is visually represented in Figure 5.13, and a sample of Lyapunov exponent is shown in Figure 5.14. We get the average value from trials:

$$\lambda_{(90,180)} = (15.5 \pm 0.7)$$

For the trials starting from  $(170^\circ, 0^\circ)$  initial angles, the trajectory divergence is visually represented in Figure 5.15, and a sample of Lyapunov exponent is shown in Figure 5.16. We get the average value from trials:

$$\lambda_{(170,0)} = (18 \pm 1)$$

The rest of the trials are added to the Appendix.

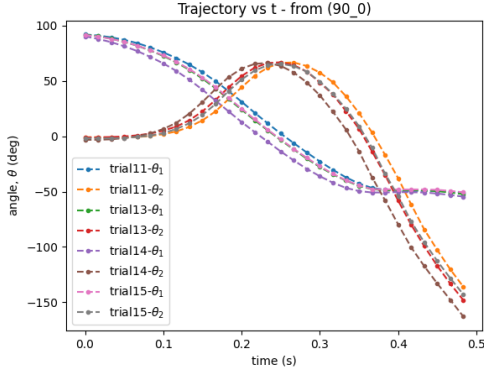


Figure 5.11: Visualizaton of trajectory divergence from  $(90^\circ, 0^\circ)$  initial angles

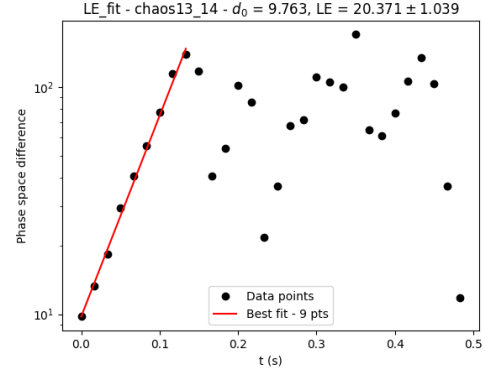


Figure 5.12: Sample of Lyapunov exponent from  $(90^\circ, 0^\circ)$  initial angles

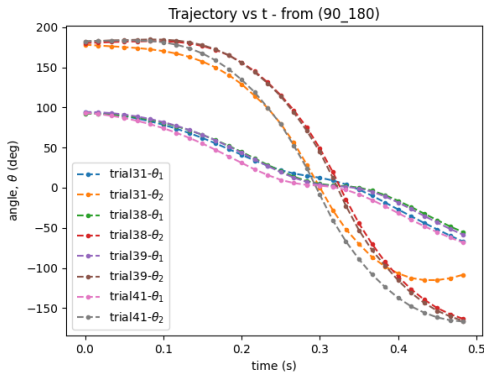


Figure 5.13: Visualizaton of trajectory divergence from  $(90^\circ, 180^\circ)$  initial angles

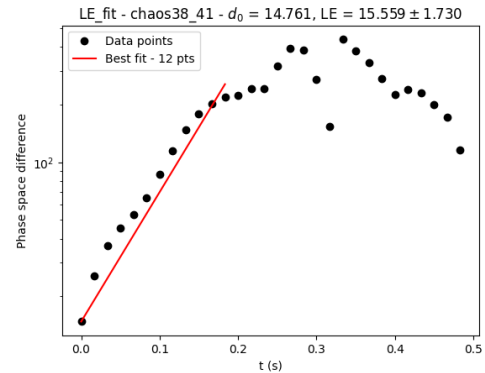


Figure 5.14: Sample of Lyapunov exponent from  $(90^\circ, 180^\circ)$  initial angles

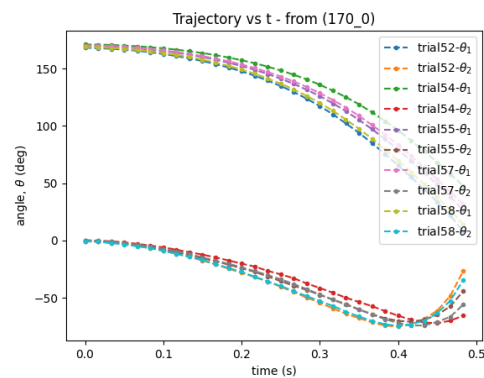


Figure 5.15: Visualizaton of trajectory divergence from  $(170^\circ, 0^\circ)$  initial angles

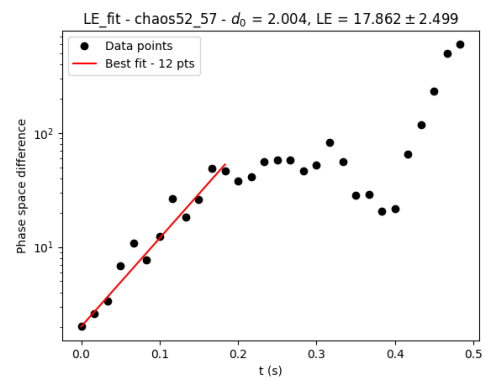


Figure 5.16: Sample of Lyapunov exponent from  $(170^\circ, 0^\circ)$  initial angles

## 5.4 Error Analysis

For the experimentally measured normal mode frequencies, we take the mean and standard deviation across different trials as the average value and its error. The error for the average value,  $\bar{\omega}$ , is thus given by:

$$\delta\bar{\omega} = \sqrt{\frac{\sum_{i=1}^N (\omega_i - \bar{\omega})^2}{N - 1}} \quad (5.1)$$

where  $N$  is the number of trials.

For the Lyapunov exponent calculated across trials, we use the weighted errors as the error within each trial is obtained through curve fit. Hence, we get the weighted average and error as follows:

$$\bar{\lambda} = \frac{\sum w_i \lambda_i}{\sum w_i} \quad (5.2)$$

$$\delta\bar{\lambda} = \sqrt{\frac{1}{\sum w_i}} \quad (5.3)$$

where the weight  $w_i = 1/\sigma_i^2$  and  $\sigma_i$  is the error associated with  $\lambda_i$ .

# Chapter 6

## Results

### Normal modes

The normal mode frequencies obtained experimentally are:

$$\omega_1 = (0.902 \pm 0.006) \text{ Hz}$$

$$\omega_2 = (1.801 \pm 0.006) \text{ Hz}$$

whereas the analytically predicted values are  $\omega_1 = 0.88$  Hz and  $\omega_2 = 1.86$  Hz. We can see that the experimentally obtained values are close to the analytically predicted values.

### Chaos

The experimentally obtained Lyapunov exponent for three different settings  $(90^\circ, 0^\circ)$ ,  $(90^\circ, 180^\circ)$ , and  $(170^\circ, 0^\circ)$  are:

$$\lambda_{(90,0)} = (20.4 \pm 0.4)$$

$$\lambda_{(90,180)} = (15.5 \pm 0.7)$$

$$\lambda_{(170,0)} = (18 \pm 1)$$

We can see that Lyapunov's exponent is positive for all three settings, indicating the chaotic behavior of the double pendulum.

# Chapter 7

## Discussions

### Why choose RK4 for solving the EoM numerically?

RK4 is one of the most popular tools in solving coupled first-order Ordinary Differential Equations (ODEs). We did contemplate using Adaptive Step-size RK4 (ASRK4), which changes the step-size according to the slope of the variables involved so that the errors in trajectories can be reduced. The advantage of ASRK4 is that it requires less computational expense without affecting accuracy.

But, for the FFT analysis, we need a stable time step, which the ASRK4 does not provide. Since we saw that the RK4 solution converges to the ASRK4 solution when we use a smaller time step, we decided to stick with RK4. Even though it took more time to complete the solution, it was manageable with our short period of analysis window and project time frame.

### Solving the problem of skipped frames in Tracker data.

For some video analysis, some frames were unable to track the position, and we found vacant spaces where the respective coordinates should have been in Tracker files. Even though we were more careful with further trials of the experiment, we added an algorithm to fill in those skipped frames by interpolating the coordinates from the neighboring frames.

With 60 frames per second captured, the isolated skipped frames can be justifiably filled this way without affecting the results. For high-speed motion in chaos analysis, we avoided skipping frames and manually added them to the Tracker software.

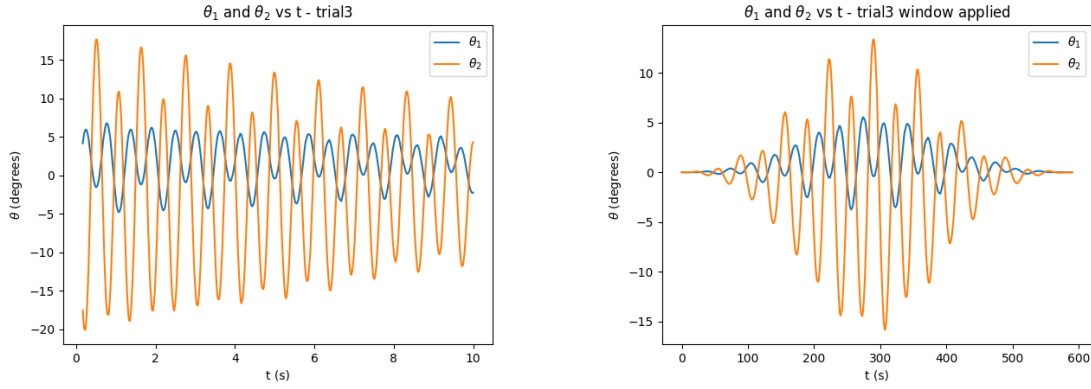


Figure 7.1: Before applying hann window

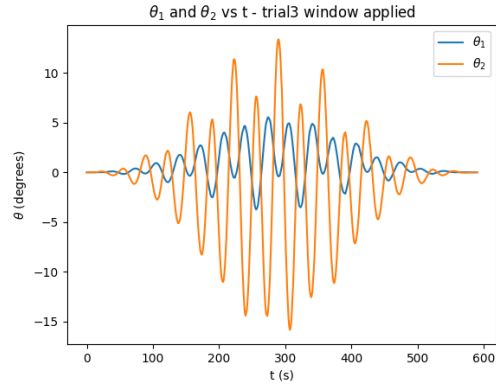


Figure 7.2: After applying hann window

### Why did we apply the Hann window before FFT analysis?

In some trials, there is a peak in zero frequency that occurs usually when the signal ( $\theta_i$  trajectory) has more area above 0 than below it. The decaying nature of the signal ( due to the decay and specific area of the signal under analysis) and any possible bias in the signal can cause this.

The naive way to approach this was to check for the second biggest peak. But on further reading, we found out that, like all shortcuts, there are some compromises involved in the FFT. The signal must be periodic in the sample window, or leakage will occur. The signal must start and end at the same point in its cycle. Leakage is the smearing of energy from the true frequency of the signal into adjacent frequencies.

To overcome this, we apply windows on the signal. Windowing reduces the amplitude of the discontinuities at the boundaries of each finite sequence. In our case, I decided to apply the Hann window (also mentioned as the Hanning window in some texts). Hann is the most commonly used window function for random signals because it provides good frequency resolution and leakage protection with fair amplitude accuracy. Hann window application on a signal is depicted in Figures 7.1 and 7.2.

### **Why only 30 frames for Tracker analysis in chaos?**

As the trajectories cannot be infinitesimally close to each other, the exponential behavior is only local and gradually transitions into non-exponential behavior over a short period. In Shibrot et al. (1992) [4], they took most consecutive points from the beginning while reducing the reduced chi-squared value  $\chi_r^2$  for the fitting to exponential form given in equation (2.13). Their experiment showed that the motions within 0.5 seconds from the beginning were only needed for the said method.

Hence, we only chose 31 frames for analysis as the frame rate is 60 per second. Among these, only 30 frames will be considered for further analysis.

### **Control of moment of release in chaos within 1 frame.**

Another control we added for the chaos analysis includes the margin of one frame (30→31) we added during analysis, which gives the freedom to pinpoint the moment of release within the first two frames which is crucial for chaos. Since we are taking the difference of trajectories, we saw that some trials showed exact exponential growth with a difference of such one frame.

### **Why make the $(\theta_1, \theta_2)$ space in $(-\infty, \infty)$ range?**

Using the `np.degrees(np.arctan2(x_1,y_1))` for finding  $\theta_1$  (or  $\theta_2$ ), we get the values in range (-180°,180°). When the  $\theta_i$  crosses this range, i.e., for example (...,-179.9,180,-179.9,...), a discontinuity can be observed in the values even though the motion was continuous.

This is fine for normal mode analysis where trajectories are well within the boundary. But in chaos analysis where the trajectory difference plays a major role, we need the  $\theta_i$  space in  $(-\infty, \infty)$  range. This gives us the proper trajectory difference, especially in cases where the trajectories cross the boundaries of the initial range (-180°,180°).

Another reason is the sudden spike of the  $\omega_i$  values at points where  $\theta_i$  crosses the boundary (-180°, 180°) as they are calculated using the gradient. There will also be a sudden spike in the  $d = |\phi_2 - \phi_1|$  when both trajectories cross the boundaries of range (-180°, 180°) at different time.

### Why adjust the space in chaos analysis for initial angle continuity?

The algorithm for implementing the above-mentioned continuity detects the spike in the trajectory and which direction the rotation is. Then, it adds and subtracts multiples of 360° to make the values continuous. See the code below.

```

1 temp_next = theta1[0] # initial angle dependent
2 for k in range(len(theta1) - 1):
3     if theta1[k+1] - temp_next > 170: #detecting +ve spike
4         add_temp -= 360
5     elif theta1[k+1] - temp_next < -170: #detecting -ve spike
6         add_temp += 360
7     temp_next = theta1[k+1]
8     theta1[k+1] += add_temp

```

As you can see, the algorithm starts the correction depending on the first value in the `theta1` list. If there is a discontinuity in the initial values, that discontinuity causes a permanent gap between trajectories. For example, (.. -179,-178,-177,..) and (..,180,181,182,..) will have a permanent gap of 360 though the trajectories are close physically.

Since the chaos analysis is only concerned with trajectory difference, the coordinate space rotation shouldn't affect the results. Hence, for any setting, we adjust the coordinate space such that the initial angles are far away from the boundary, ensuring continuity. As (90,0) and (170,0) initial angles are safe in the (-180,180)  $\theta$  range, we only needed to rotate coordinates for the (90,180) setting.

## 7.1 Sources of error

- Distortion of coordinates due to limitations of the camera lens and field of vision.
- High angular velocity observed during chaotic motion causes the individual frames in the video to be blurry and causes errors in detecting marker positions.
- The action of releasing the pendulum may add external momentum to the system by accident.
- The same position of release or proximity between two trials in chaos analysis cannot be ensured due to the manual release of the pendulum.

## 7.2 Precautions

Several precautions were observed during the experiment, including:

- To reduce distortion of coordinates in the video captured, the camera should be placed directly in front of the system at a perpendicular angle and in a stable position.
- Ensuring visibility of markers: It is essential to confirm that the markers on the arms of the pendulum are clearly visible while capturing videos.
- Maintaining consistency in initial angles: For the chaotic scenarios, it is essential to ensure that the initial angles do not undergo drastic changes between each trial.
- To capture the high-speed chaotic motion, we can use a camera device with higher capability. In our case, we manually input the position in the middle of the smeared marker trail in individual frames. Since only 30 frames were under analysis, this was manageable.

- We release the pendulum carefully, avoiding any sudden movement. Another aluminum structure for ensuring proper release has been suggested and is planned for subsequent lab use.
- Caution regarding the secondary arm of the pendulum, which can reach high angular velocities, posing a risk of injury. It is crucial to ensure that no body parts are in proximity when the pendulum is in motion, particularly during chaotic cases.

# Chapter 8

## Conclusions

In summary, this experiment thoroughly explored the complex dynamics of the double pendulum system through a comprehensive blend of experimental and theoretical methodologies. The investigation covered a spectrum of experiments, examining normal mode frequencies and the Lyapunov exponent under various initial conditions. Additionally, numerical methods were also utilized to solve the system's equations of motion.

For the normal mode analysis, we saw that the experimentally obtained frequencies were very close to the analytically predicted frequencies. We also observed the combination of the normal modes in an arbitrary small-angle motion. The linear behavior of the system was clearly observed in this case.

For the study of a double pendulum starting from large angles, we saw a steady positive Lyapunov exponent for all three settings we studied which clearly indicates the chaotic behavior in the system.

Since the EoM we used is based on a simplified structure and various assumptions, a more detailed analysis of the complex structure, related Moments of Inertia, or fewer assumptions could possibly bring us closer between the prediction and observation. This can be achieved using proprietary software like SolidWorks or some CAD software. There is also the possibility of studying the system under various external forces, tilting the system, or adding damping through change of medium, etc.

# References

- [1] R. B. Levien, S. M. Tan. 1993. Double pendulum: An experiment in chaos. *Am. J. Phys.* 61 (11). 1038–1044.
- [2] A. D. Myers, J. R. Tempelman, D. Petrushenko, F. A. Khasawneh. 2020. Low-cost double pendulum for high-quality data collection with open-source video tracking and analysis. *HardwareX*, 8, e00138. <https://doi.org/10.1016/j.hwx.2020.e00138>
- [3] D. Brown, R. Hanson, and W. Christian, Computer Program TRACKER VIDEO ANALYSIS AND MODELING TOOL, Version 6.1.5 (2023), WWW Document, (<https://physlets.org/tracker/>).
- [4] T. Shinbrot, C. Grebogi, J. Wisdom, J. A. Yorke. 1992. Chaos in a double pendulum. *Am. J. Phys.* 60 (6). 491–499. <https://doi.org/10.1119/1.16860>

# Appendix A

The chaos trial numbers might seem bizarre as the trial numbers were chosen in sets like (11-15), (31-41), and (51,59) for easier identification. Many trials were discarded due to the previously mentioned experimental errors with the position and way of pendulum release. The rest were analyzed in combinations within their settings and analyzed for Lyapunov's exponent.

The rest of the experimental results are given here for reference.

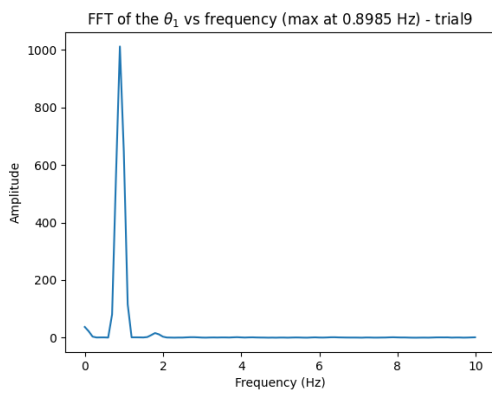


Figure A.1: NM1 trial 1 FFT

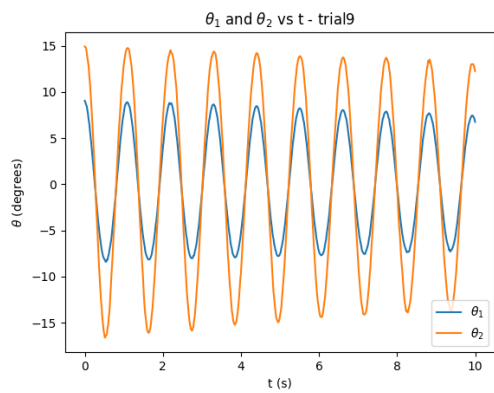


Figure A.2: NM1 trail 1 trajectory

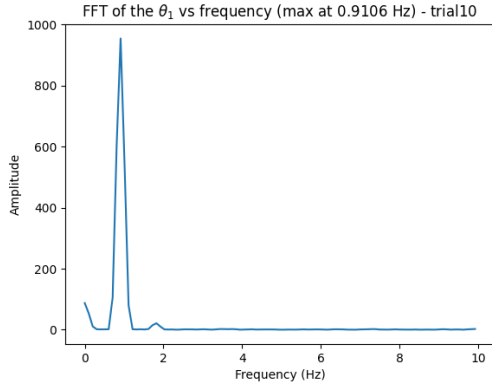


Figure A.3: NM1 trial 2 FFT

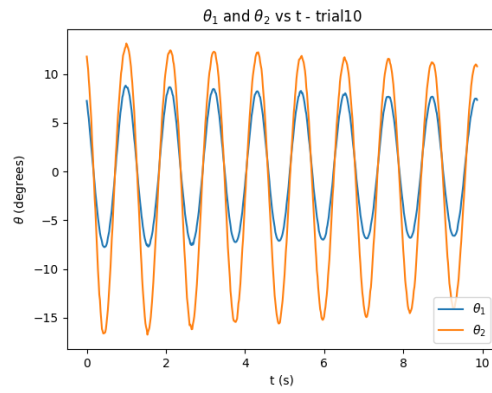


Figure A.4: NM1 trial 2 trajectory

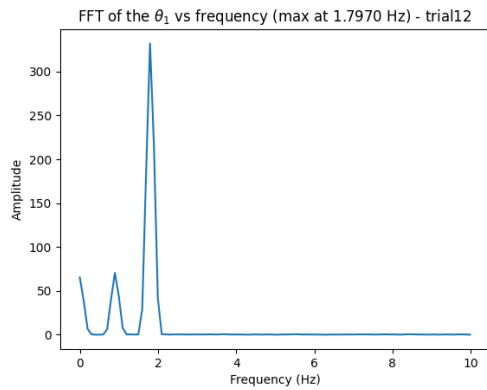


Figure A.5: NM2 trial 1 FFT

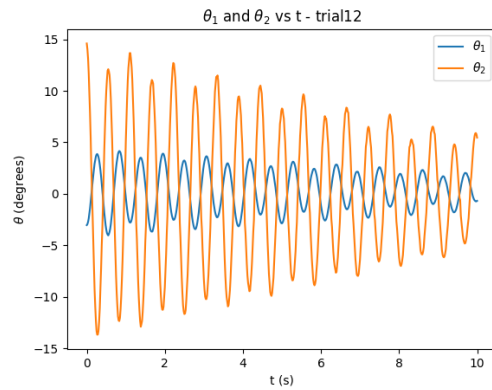


Figure A.6: NM2 trial 1 trajectory

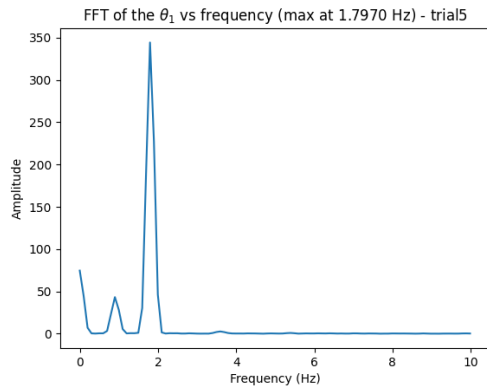


Figure A.7: NM2 trial 2 FFT

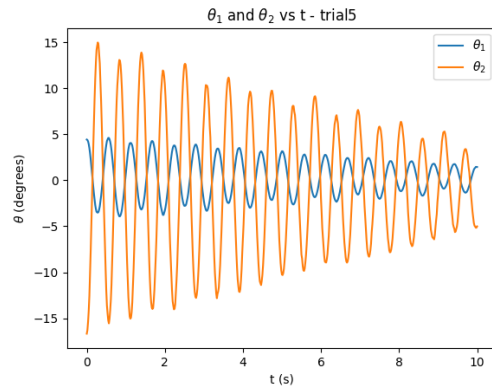
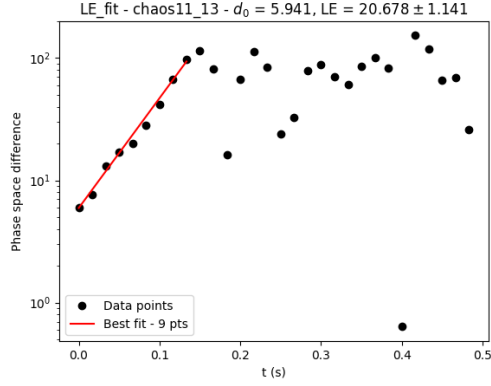
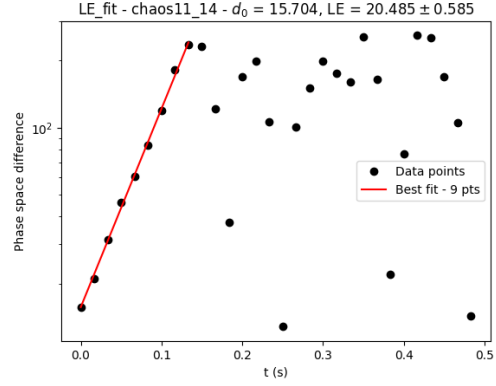
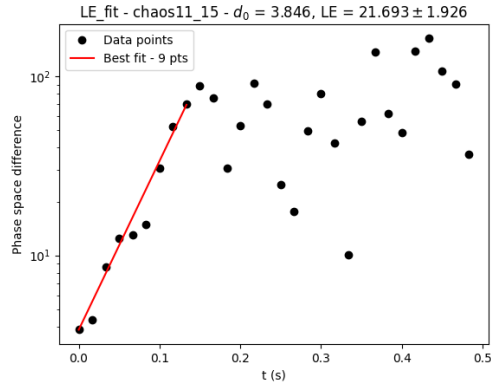
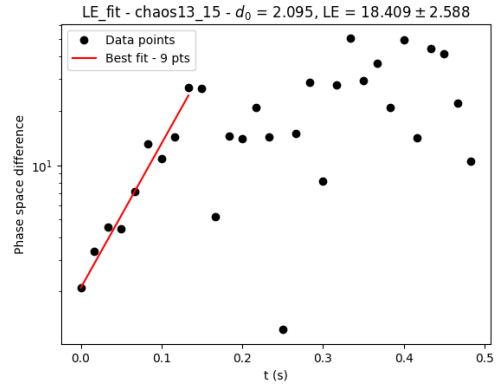
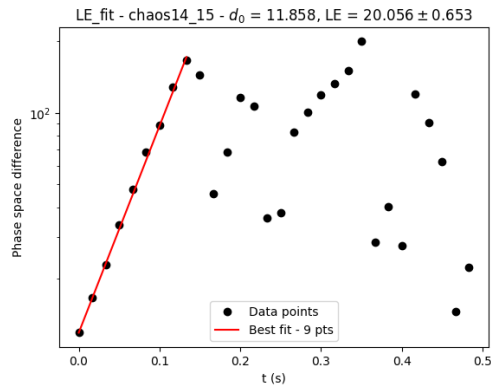
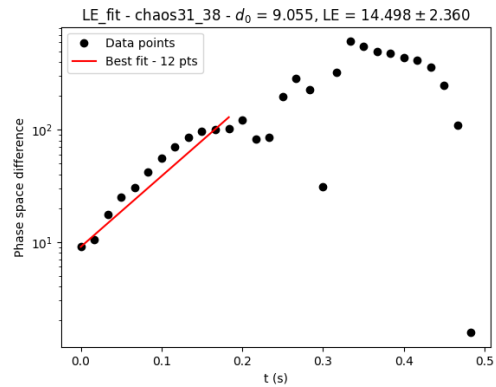
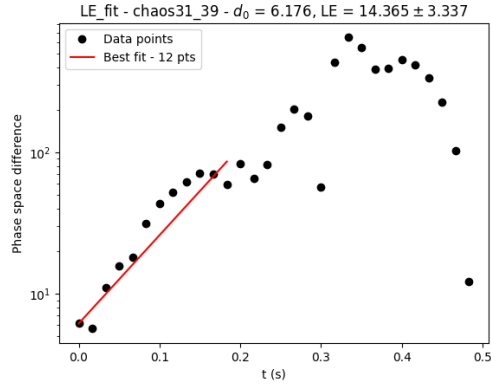
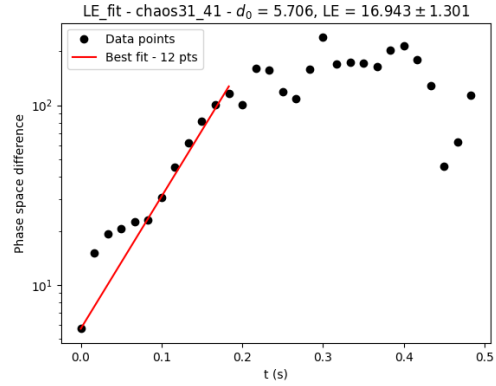
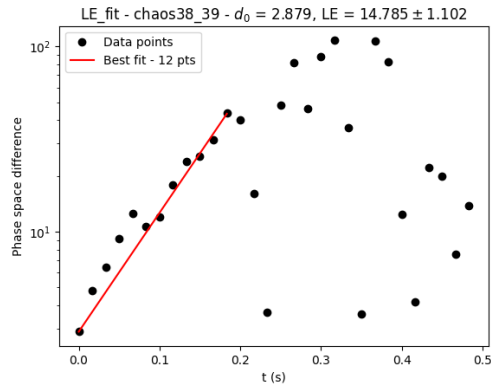
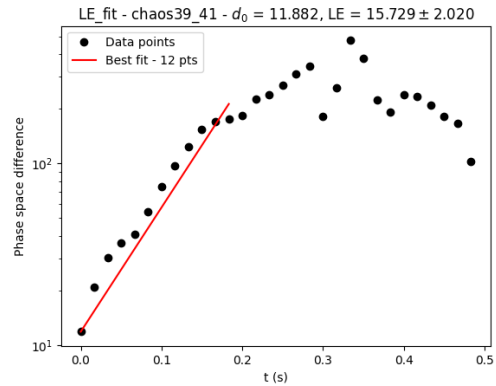
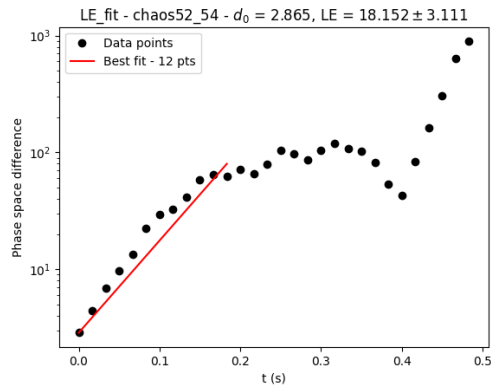
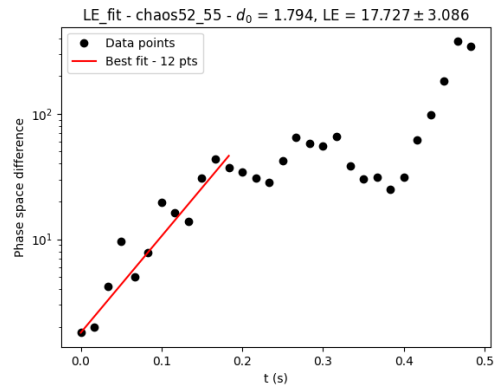
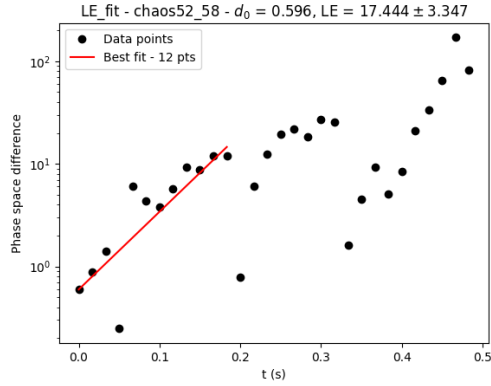
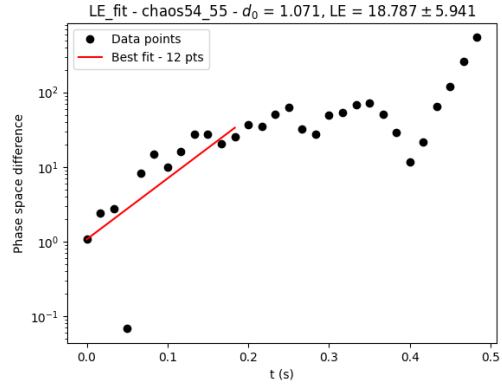
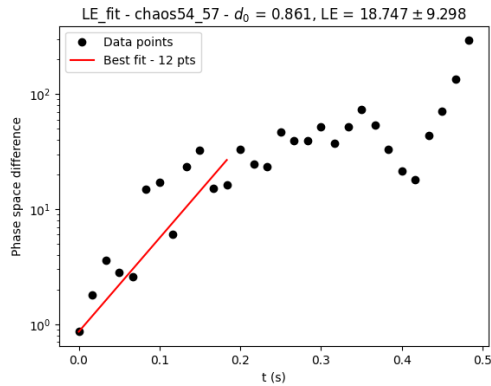
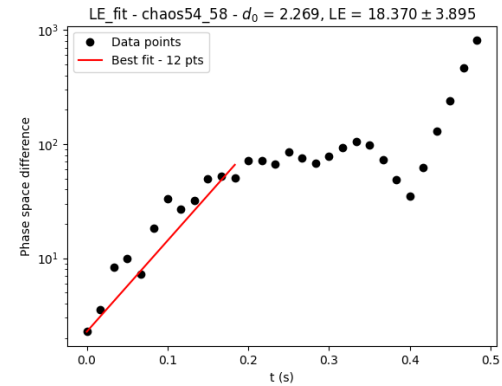
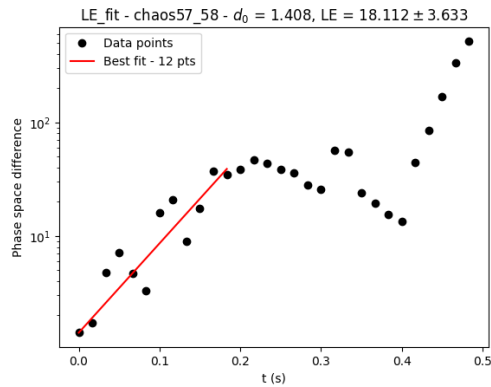


Figure A.8: NM2 trial 2 trajectory

Figure A.9:  $(90^\circ, 0^\circ)$  trial 11 vs 13Figure A.10:  $(90^\circ, 0^\circ)$  trial 11 vs 14Figure A.11:  $(90^\circ, 0^\circ)$  trial 11 vs 15Figure A.12:  $(90^\circ, 0^\circ)$  trial 13 vs 15Figure A.13:  $(90^\circ, 0^\circ)$  trial 14 vs 15Figure A.14:  $(90^\circ, 180^\circ)$  trial 31 vs 38

Figure A.15:  $(90^\circ, 180^\circ)$  trial 31 vs 39Figure A.16:  $(90^\circ, 180^\circ)$  trial 31 vs 41Figure A.17:  $(90^\circ, 180^\circ)$  trial 38 vs 39Figure A.18:  $(90^\circ, 180^\circ)$  trial 39 vs 41Figure A.19:  $(170^\circ, 0^\circ)$  trial 52 vs 52Figure A.20:  $(170^\circ, 0^\circ)$  trial 52 vs 55

Figure A.21:  $(170^\circ, 0^\circ)$  trial 52 vs 58Figure A.22:  $(170^\circ, 0^\circ)$  trial 54 vs 55Figure A.23:  $(170^\circ, 0^\circ)$  trial 54 vs 47Figure A.24:  $(170^\circ, 0^\circ)$  trial 54 vs 58Figure A.25:  $(170^\circ, 0^\circ)$  trial 57 vs 58